LETTER • OPEN ACCESS

A Kirigami shape memory polymer honeycomb concept for deployment

To cite this article: Robin M Neville *et al* 2017 *Smart Mater. Struct.* **26** 05LT03

View the article online for updates and enhancements.

Related content

- Origami-inspired active structures: a synthesis and review
  Edwin A Peraza-Hernandez, Darren J Hartl, Richard J Malak Jr et al.

- Natural fibres actuators for smart bio-inspired hygromorph biocomposites
  Antoine Le Duigou, Samuel Requile, Johnny Beaugrand et al.

- Self-Expanding/Shrinking Structures by 4D Printing
  M Bodaghi, A R Damanpack and W H Liao

Recent citations

- Shape-matching soft mechanical metamaterials
  M. J. Mirzaali *et al*

- The mechanical design of a hybrid intelligent hinge with shape memory polymer and spring sheet
  Changguo Wang and Yafei Wang

- Numerical study of smart honeycomb core using shape memory polymers
  Ran Tao *et al*

Letter

A Kirigami shape memory polymer honeycomb concept for deployment

Robin M Neville[1], Jianguo Chen[2], Xiaogang Guo[2], Fenghua Zhang[2], Wenxin Wang[2], Yousef Dobah[1], Fabrizio Scarpa[1], Jinsong Leng[2] and Hua-Xin Peng[3]

[1] Advanced Composites Centre for Innovation and Science (ACCIS), University of Bristol, Queens Building, University Walk, BS8 1TR Bristol, United Kingdom
[2] Center for Composite Materials and Structures, HIT Science Park, Harbin Institute of Technology, Harbin 150080, People's Republic of China
[3] Institute for Composites Science Innovation (InCSI), Zhejiang University, 38 Zheda Road, Hangzhou 310027, People's Republic of China

E-mail: robin.neville@bristol.ac.uk

Abstract

We present a shape memory polymer (SMP) honeycomb with tuneable and shape morphing mechanical characteristics. Kirigami (Origami with cutting allowed) techniques have been used to design and manufacture the honeycomb. The cellular structure described in this work has styrene SMP hinges that create the shape change and the deployment actuation. To create a large volumetric deployment, the Kirigami open honeycomb configuration has been designed by setting an initial three-dimensional re-entrant auxetic (negative Poisson's ratio) configuration, while the final honeycomb shape assume a convex (positive Poisson's ratio) layout. A model was developed to predict the shape change of the structure, and compared to experimental results from a demonstrator honeycomb deployment test.

Keywords: shape memory polymer, deployable structures, honeycomb, morphing structures

(Some figures may appear in colour only in the online journal)

1. Introduction

Origami engineering has been branded as one of the most promising multiscale design methods to produce structures and materials with unusual deformation mechanisms and shape changing characteristics. Origami tessellations have been used to develop deployable structures for space applications [1–3]. Other applications of Origami have ranged for example from corrugated cores [4–6] to stents designs [7], micro-assembly and robotics [8, 9] and graphene technology [10]. All these applications are compounded by the use of several mathematical frameworks that allow to design the engineering applications from first principles [11–14]. Kirigami is the ancient Japanese art of cutting and folding paper, a process that shapes a two-dimensional sheet into a three-dimensional structure. The use of cutting allows Kirigami to create honeycombs and other porous cellular configurations. Kirigami has been recently adopted to develop shape changing smart materials and morphing components [15, 16], multiscale structures with unusual deformation mechanisms [17, 18], soft robotics [16], high-performance cores for sandwich structures [19, 20], metamaterials for wave propagation [21, 22] and new classes of nanocomposite materials [23–25]. The first known instance of Kirigami being used to create a honeycomb is a patent filed by Dean in 1921 [26].
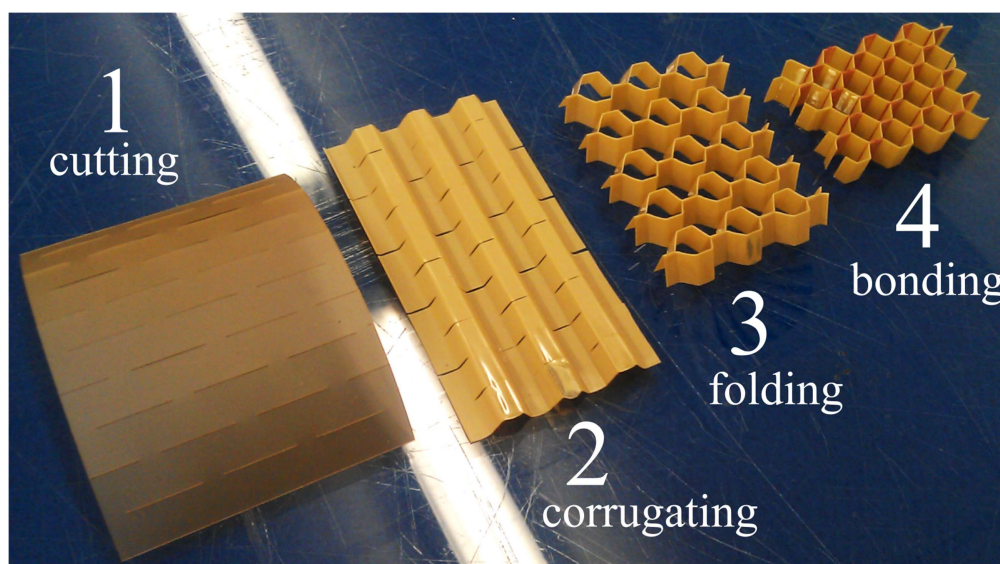
Figure 1. The Kirigami honeycomb manufacturing process. The specimens shown here were made of PEEK sheet as part of some of the Authors' past work [29].

Figure 1 shows the method proposed in the patent, which involves the use of cutting, corrugating, folding, and bonding steps. A hexagonal honeycomb configuration can be made from adopting Kirigami techiques because cuts in the sheet open up into hexagonal holes and therefore create the cells. Nojima and Saito have developed a mathematical framework that links the cutting pattern to the final hexagonal honeycomb geometry [27]. The dimensions of the cutting pattern on a 2D sheet material are directly related to the final dimensions of the 3D structure, and quite simple changes in the cutting pattern can generate significant changes in the 3D geometry. Saito *et al* have provided a thorough explanation about how the cutting pattern affects the honeycomb geometry and related manufacturing methods [28]. It is also possible to vary the thickness within the honeycomb, which can give rise to some secondary functions.

In past works some of the Authors have adapted Nojima and Saito's methods to develop a new class of cellular structures with high flexibility in terms of final geometry [29, 30]. These structures are called 'open' honeycombs because they lack a closed cell topology. The behaviour of these structures is significantly affected by the presence of folds within the cellular configuration. Variations in the fold angle produce large volume changes (see figure 2). The flexibility and volume variation of these cellular structures could be exploited for general space or mechanical deployable structures. The aim of this work is to create an open honeycomb using shape memory polymers (SMPs) in such a way that the folds can be actuated by thermal loading, and can therefore create a controllable shape changing configuration.

SMPs are polymers that can retain different shapes, and can be triggered to move between these states by certain stimuli. SMPs are emerging as an alternative to SMAs. In contrast to SMAs, SMPs generate small stresses (1–3 MPa), large strains (up to 800%), and are significantly easier to process and customise [31].

SMPs have been widely used for applications related to shape morphing. Liu *et al* [31] provide a good general summary of use of SMPs in this area, with polymers being categorised into different classes based on their composition and activation mechanisms. The polymer used in this work falls into category 1—chemically cross-linked glassy thermosets. In this type of SMP the glass transition temperature (T_g) serves as the transition for the shape memory effect. This results in a one-way shape memory action i.e. a one-time transition from a 'learned' temporary shape back to the as-manufactured permanent form. Because the permanent shape is fixed by covalent bonding, the permanent form must be set during the manufacture of the polymer by a process like casting. The polymer can then be 'taught' a temporary shape by thermoforming above its T_g, and it can be returned to its permanent shape again by heating above its transition temperature. SMPs are currently developed for a wide variety of applications, from general morphing structures [32], self-healing [33], smart mandrels [34], 3D printing [35] to damping [36] and viscoelastic/reversible adhesion [16].

Examples of use of shape memory materials in honeycomb structures is fairly limited. Hassan *et al* [37] have manufactured and characterised one of the first shape memory honeycombs made from SMA strips ($Ni_{48}Ti_{46}Cu_6$). Other works about the development of honeycombs and cellular structures with different types of SMA materials and geometry can be found in [38–41]. A shape memory alloy cellular structure that exploits the auxetic nature of the chiral configuration has been also developed to create a deployable demonstrator [42] and space antenna [43]. Rossiter *et al* [44] have also produced a deployable chiral honeycomb, this time using SMP (CRG Veriflex laminate) to achieve greater deployment strains and lower density and metastable configurations. Auxetic materials are materials which can expand in all directions [45, 46], and as a result they are often used
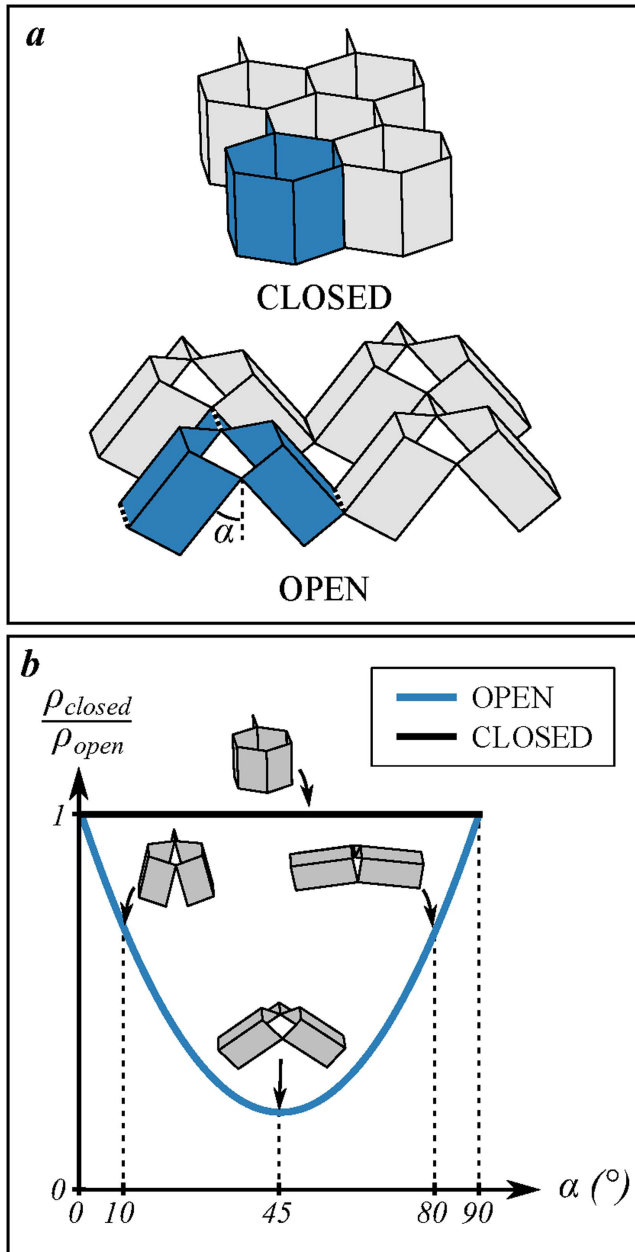
Figure 2. The density of open honeycombs compared to traditional closed honeycombs. (a) An open honeycomb compared to its closed counterpart. The unit cell of each configuration is shown in colour. Folds are shown by dashed lines. The fold angle α is measured from the vertical. (b) A schematic graph of the volume change of open honeycombs with fold angle α (redrawn from [29]). The unit cell of the honeycomb is shown at key points to illustrate the shape change. The relative density of the open honeycomb is given by $\frac{\rho_{\text{open}}}{\rho_{\text{closed}}} = \frac{1}{C \sin 2\alpha + 1}$ where C is a function of the fixed cell dimensions.

for deployable structures. We use an auxetic honeycomb configuration in this work for the same reason.

One of the most important characteristics of deployable structures is their capability of deploying or assembling in an autonomous fashion. Self-folding origami is very relevant to this work because it also deals with the self-assembly of sheet-type materials. Hawkes *et al* [47] have created a programmable sheet capable of assuming two different folded

states. They prescribed a triangular 'crease pattern' by embedding rigid triangles into a silicone sheet, such that the original planar configuration could fold only along the silicone lines. To this extent they have used SMA actuators to control folding and embedded magnets have been used to hold the folds closed after actuation. While the sheet successfully forms the two folded shapes, this approach poses several problems. The manufacturing process is complicated and requires many steps, and each fold requires an individual actuator which must be heated individually, and therefore the sheet must also include heating elements and wiring to activate the shape change. Felton *et al* [48] have developed an alternative approach for fold actuation, consisting of producing composite specimens with layers made from paper substrates, SMP and polyimide. The paper layer was scored with the crease pattern. Resistive circuits etched onto the polyimide layer were used to locally actuate the SMP. The asymmetry of the laminate causes the sheet to fold when the SMP contracts, and the inclusion of the SMP actuator and the circuitry as single sheets results in a much simpler manufacturing process compared to the one used by Hawkes *et al* [47]. This approach could allow the creation of much larger structures, also to be stored in a flat state prior to use. Tolley *et al* [49] have further developed this type of technology focusing more on the control of the final shape of the structure. In [49] a similar laminate approach is used but without the polyimide layer; SMP-paper laminates are simply heated in a uniform manner. Tolley and co-workers present a method for limiting the deflection of a fold, such that the final shape of the structure can be precisely controlled. They also present a technique to self-seal the structures to be locked in place after folding. New types of folding mechanisms triggered by multi-temperature T_{g}s SMPs with differential elasticity and plasticity have been also recently developed and proposed by Zhao and co-workers [50].

The problem with all the above-mentioned self-folding approaches is that the structure starts as a flat sheet. This configuration can be undesirable for specific structural and stowage applications because the flattened structure takes up a significant amount of space. In this work we aim to create a structure with shape memory polymer material with a small folded initial configuration, which deploys to a larger final state. The structure takes also advantage of a morphing open honeycomb configuration, that creates by geometry Poisson's ratio switch effects and variable stiffness configurations [29, 30].

2. Analytical modelling

2.1. Dimensions and volume change

In this section we present the analytical formulas that describe the dimensions of the honeycomb, subjected to changes in the fold angles α and θ. We adapt the calculations from [29] to take into account the thickness of the cell walls, because the latter has a significant effect on the dimensions of the honeycomb in its folded state.
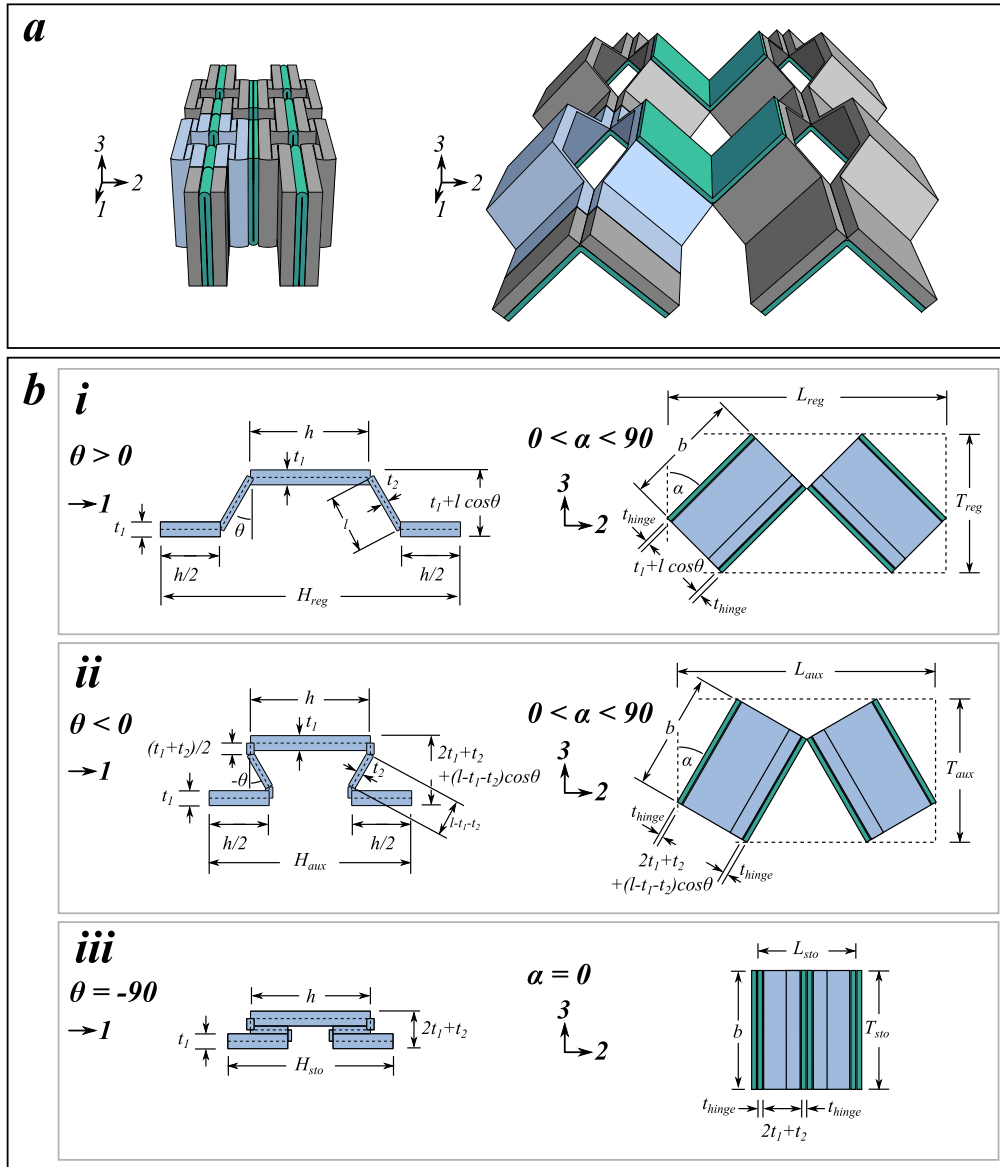
Figure 3. Stowed and deployed honeycomb dimensions. (a) Left: the honeycomb in its reentrant stowed configuration. Right: the honeycomb in its non-reentrant deployed configuration. The strip components are shown in grey, with unit cell highlighted blue. Hinges are shown in green. (b) Detail views of the unit cell, showing dimensions H, L, T, for different configurations. (i) The regular (non-reentrant) configuration where $\theta > 0$. (ii) The auxetic (reentrant) configuration where $\theta < 0$. Because the thickness of the strip is significant, we assume that a piece of the l-wall (of length $(t_1 + t_2)/2$) is consumed in the strip fold. (iii) The stowed configuration. This is the auxetic configuration with $\theta = \alpha = 0$.

In order to achieve expansion along all the directions we use an auxetic (negative Poisson's ratio) re-entrant configuration for the stowed state, which will deploy into a regular non-auxetic deployed phase (see figure 3(a)). Figure 3 also shows the dimensions of the unit cell along the 1, 2, 3 directions for both the auxetic and regular configurations. The dimensions H, L, T are given by equations (1).

$$H_{\text{reg}} = 2h + 2l \sin \theta, \tag{1a}$$

$$L_{\text{reg}} = 2b \sin \alpha + 2(l\cos \theta + t_1 + 2t_{\text{hinge}})\cos\alpha, \tag{1b}$$

$$T_{\text{reg}} = b\cos \alpha + (l\cos \theta + t_1 + 2t_{\text{hinge}})\sin \alpha, \tag{1c}$$

$$H_{\text{aux}} = 2h + 2(l - t_1 - t_2)\sin \theta, \tag{1d}$$

$$\begin{aligned} L_{\text{aux}} = 2b \sin \alpha + 2(2t_1 + t_2 + 2t_{\text{hinge}} \\ + (l - t_1 - t_2)\cos \theta)\cos \alpha, \end{aligned} \tag{1e}$$

$$\begin{aligned} T_{\text{aux}} = b\cos \alpha + (2t_1 + t_2 + 2t_{\text{hinge}} \\ + (l - t_1 - t_2)\cos \theta)\sin \alpha, \end{aligned} \tag{1f}$$

These unit cell dimensions can be used to represent an infinite honeycomb, but for a finite cellular structure we must adapt these formulas to take into account edge conditions (e.g. no hinges are attached on the outsides of the honeycomb, and the outermost h-walls are slightly longer). For a honeycomb with number of cells N_1 and N_2 along the 1

Table 1. Honeycomb dimensions.

Dimension	Value
h	20 mm
l	10 mm
θ	30°
t_1	2.5 mm
t_2	1.25 mm
b	25 mm
t_{hinge}	1 mm
α_{sto}	0°
α_{dep}	45°
θ_{sto}	−90°
θ_{dep}	30°

and 2 directions, from inspection one can derive the honeycomb dimensions: (2).

$$H_{\text{aux}}^* = N_1 H_{\text{aux}} + h, \tag{2a}$$

$$L_{\text{aux}}^* = N_2 L_{\text{aux}} - 2t_{\text{hinge}} \cos \alpha, \tag{2b}$$

$$T_{\text{aux}}^* = T_{\text{aux}}, \tag{2c}$$

$$H_{\text{reg}}^* = N_1 H_{\text{reg}} + h, \tag{2d}$$

$$L_{\text{reg}}^* = N_2 L_{\text{reg}} - 2t_{\text{hinge}} \cos \alpha, \tag{2e}$$

$$T_{\text{reg}}^* = T_{\text{reg}}. \tag{2f}$$

Table 1 shows the dimensions for the SMP deployable honeycomb used in this work. These can be substituted into (2) to predict the stowed and deployed dimensions of the manufactured cellular structures. The dimensions used in this work were selected to easily produce a working demonstrator. The honeycomb cell dimensions are indeed quite large to reduce the impact of manufacturing tolerances. However, the model presented in this work is not limited to the dimensions used here, but could be extended to prototypes with different dimensional values. The limiting factor on scaling is most likely provided by the material thickness. For example, if the structure is scaled up several times its current size the designer will eventually encounter problems folding the resulting very thick hinges. Similarly, the scaling down will eventually lead to the material becoming too thin for classical macroscale engineering applications. Other factors which could also make the model less valid are: (a) the combinations of dimensions that cause the walls to self-intersect (i.e., an un-manufacturable geometry) and (b) large changes in one dimension compared to the others, which could cause a very elongated geometry of the honeycomb.

2.2. Hinge moment

In this section we estimate the opening moment generated by the SMP hinge. The hinges are manufactured in the deployed position, and must be thermoformed into the stowed configuration. During thermoforming an applied moment M_{ext} produces a stress distribution σ_θ through the thickness of the hinge. We use an engineering curved beam theory model [51]

to model the hinge, with figure 4 showing the curved beam geometry considered. The stress distribution due to bending and the location of the neutral axis can be described by equations (3) and (4).

$$\sigma_\theta = -\frac{M_{\text{ext}} y}{Aer}, \tag{3}$$

$$e = R - r_n. \tag{4}$$

When the hinges are activated and the strain is recovered we assume that the distribution of the SMP activation strength σ_a is the same as the distribution of the stored stress σ_θ. The shape memory polymer generates a hinge opening moment equal to M_{ext}—i.e.: $\sigma_\theta = \sigma_a$ and $M_{\text{ext}} = M_{\text{smp}}$. Substituting this into (3) we obtain:

$$M_{\text{smp}} = -\frac{Aer\sigma_a}{y}. \tag{5}$$

From figure 4 it can be seen that $y = r_n - r$, and we substitute this into (5) to obtain:

$$M_{\text{smp}} = -\frac{Aer\sigma_a}{r_n - r}. \tag{6}$$

We use table 9.1 from [51] with $R = 0.6$ mm and $c = d/2 = 0.5$ mm to obtain $e = 0.183$ mm. We then substitute e into (4) to obtain $r_n = 0.417$ mm. $A = h\, t_{\text{hinge}} = 20$ mm². We assume that the maximum tensile strength σ_a on the convex face is equal to the measured activation strength σ_a of the SMP, and therefore we substitute $r = R + c = 1.1$ mm into (6) to obtain:

$$M_{\text{smp}} = 5.895\, \sigma_a. \tag{7}$$

From these calculations it is evident that M_{smp} is very much dependent on the hinge thickness and the position of the neutral axis.

3. Prototype, results and discussions

3.1. SMP honeycomb manufacturing

The particular SMP used in this work consists of a styrene-based polymer synthesised by mixing styrene and butyl acrylate with benzoyl peroxide and cross-linking agent divinylbenzene, followed by stirring at room temperature (further details can be found in [52]). The glass transition temperature of the polymer is ($T_g \approx 70\,°C$) and serves as the shape memory transition temperature. The shape memory action is a one-time transition from a 'learned' temporary shape back to the as-manufactured permanent shape. To create a deployable SMP honeycomb, we used the SMP's permanent shape for the deployed configuration, and the temporary shape for the stowed phase. Heating of the stowed configuration would cause it to return to its deployed configuration. A casting process was used to fix the honeycomb deployed shape during the cure of the polymer. The mixture of styrene, butyl acrylate, benzoyl peroxide and divinylbenzene was poured into moulds and cured at 75 °C for 24 h. To simplify the
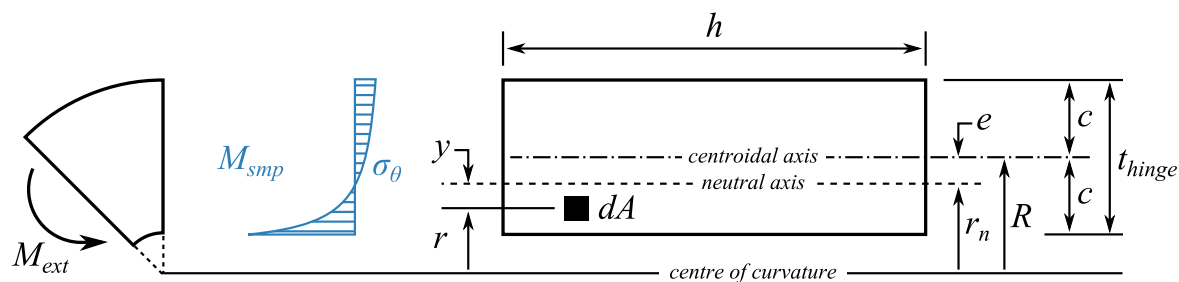
Figure 4. Curved beam geometry (adapted from [51]). An external moment M_{ext} is applied to the curved beam. This generates the circumferential stress distribution σ_θ. M_{smp} is the hinge opening moment generated by the activation of the SMP.
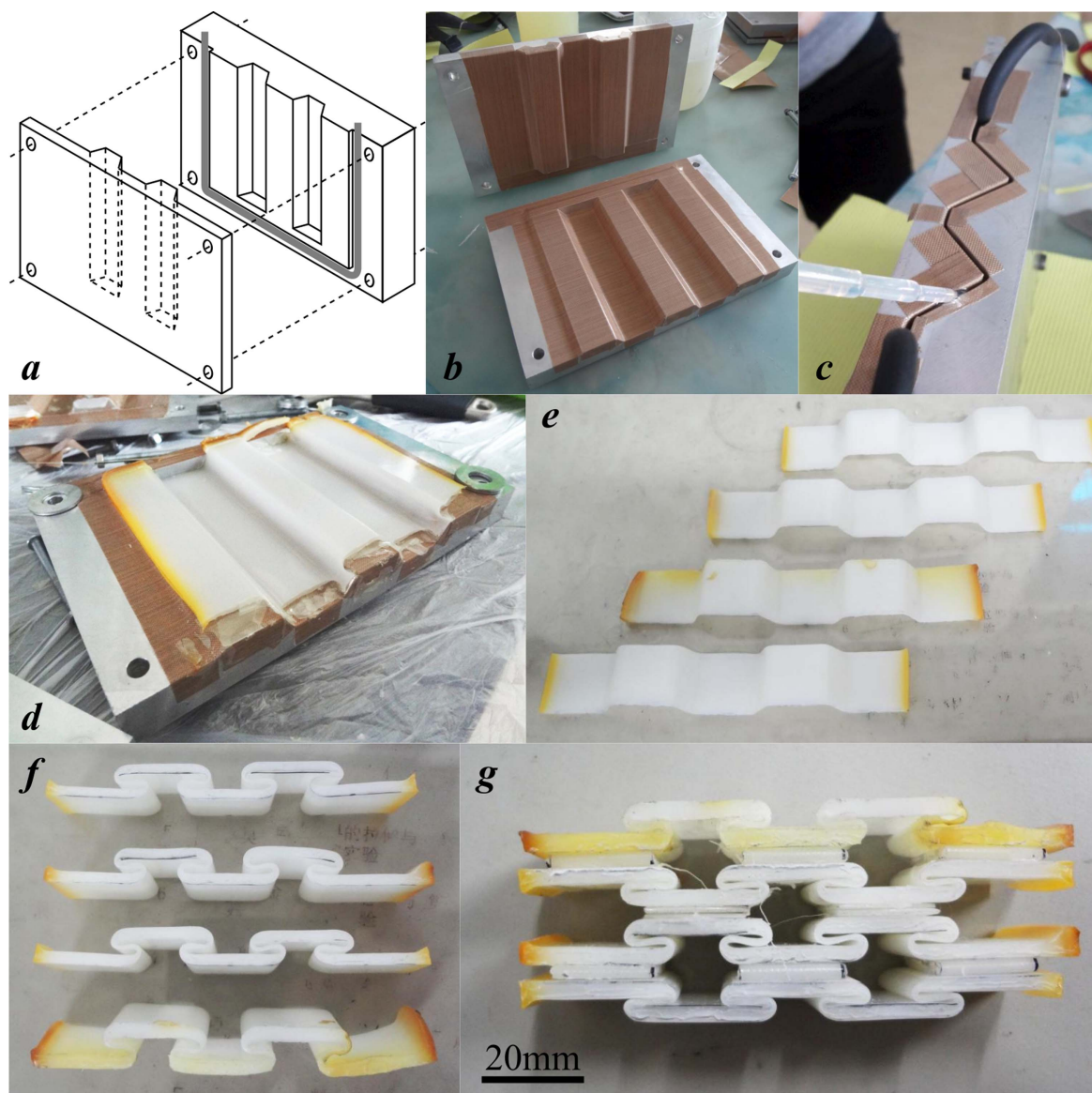

Figure 5. The manufacturing process used to produce the SMP honeycomb. (a) A diagram of the moulds used to form the strip components. The moulds are aligned and held closed by bolts, and washers are used to control the thickness of the component. Rubber tubing (grey line) is used to seal the working section. (b) The working section of the strip moulds is coated with release film. (c) Uncured SMP is poured into the closed hinge moulds before being cured at 75 °C for 24 h. (d) The cured part is removed from the strip moulds. (e) The cured part is cut into strips. (f) The components are thermoformed into their stowed shape. (g) The stowed strips and hinges are bonded using cyanoacrylate adhesive to form the stowed honeycomb.
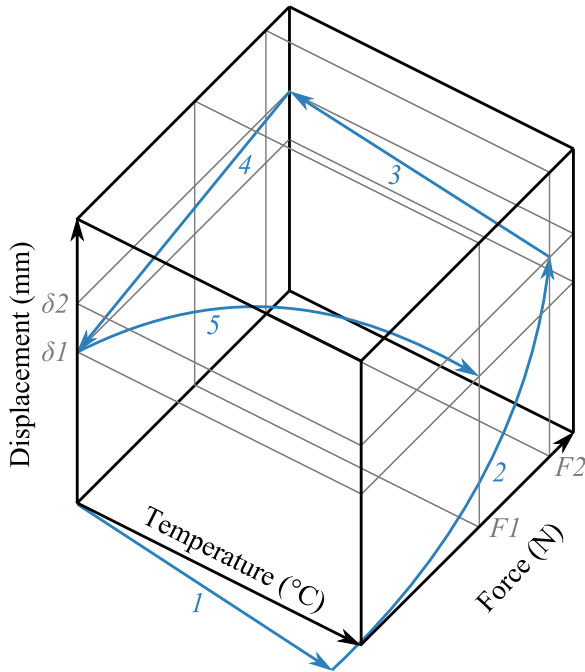
Figure 6. A schematic of the activation strength experiment in force/displacement/temperature space. (1) The specimen was heated to $T = 80\,°C$ while held at constant displacement. Thermal expansion of the specimen caused a small compressive load. (2) The temperature was held constant at $T = 80\,°C$ while the specimen was stretched to $\delta_2 = 20$ mm at a constant rate of 5 mm/min. Force was measured. (3) The specimen was held at constant $\delta = \delta_2$ and cooled to room temperature. This fixed the temporary shape of the SMP. (4) At room temperature, the specimen was released from the machine grips to release any elastic strain ($\delta_2 - \delta_1$). (5) The specimen was reinserted into the grips and heated to $T = 80\,°C$ at a rate of $10\,°C\,min^{-1}$ while held at constant $\delta = \delta_1$. The recovery force $F1$ generated by the specimen was measured.

moulds, the honeycomb was split into strip and hinge components (see figure 3(a)). The hinges and strips were thermoformed into their stowed configurations and subsequently assembled to form the stowed honeycomb. Figure 5 shows the manufacturing process in detail.

3.2. Activation force measurement

To estimate the hinge moment generated by the SMP hinges the activation strength of the SMP was determined experimentally using the procedure described in figure 6. An Instron tensile test machine with a temperature controlled chamber (500 N load cell) was used to heat rectangular SMP coupons and measure the activation force generated by the shape memory action. The activation strength is then given by $\sigma_a = F_a/A$. Six specimens were tested, using a strain rate of $5\,mm\,min^{-1}$ for the stretching phase, and a heating rate of $10\,°C\,min^{-1}$ for the recovery phase. The mean value of the activation strength across the whole sample population was 0.49 MPa, with a standard deviation of 0.118 MPa. We substitute the measured σ_a into (7) to predict a final hinge moment $M_{smp} = 2.89$ Nmm.
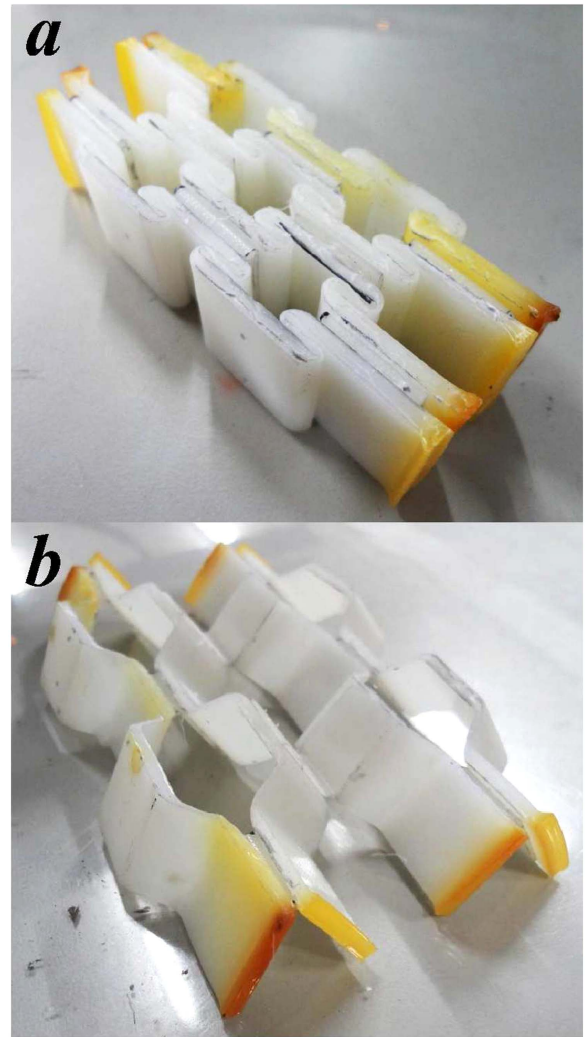

Figure 7. (a) Stowed configuration and (b) deployed configuration of the SMP honeycomb.

3.3. SMP honeycomb deployment experiment

We performed a deployment test of the SMP honeycomb demonstrator to measure the volume of the deployed state relative to the stowed configuration, and compare the volume change to the one provided by the theoretical prediction. The stowed configuration was heated to 100 °C using the test machine temperature chamber, and deployment was observed. When no further movement was recorded, the honeycomb was removed from the chamber and the dimensions H, L, and T were measured using Vernier calipers (several measurements were taken per dimension and averaged). Plates were placed under and over the honeycomb to gain a flat surface in order to measure the thickness. Figure 7 shows the stowed and fully deployed configurations.

Figure 8 shows the experimental results compared to the analytical predictions. It is evident that the stowed volume was larger than expected, while the deployed volume showed a lower deployment ratio ($\approx20\%$). It is also possible to observe that both the H and L dimensions were slightly larger than predicted in the stowed configuration ($\approx2\%$), indicating that the thermoformed state was not completely uniform and
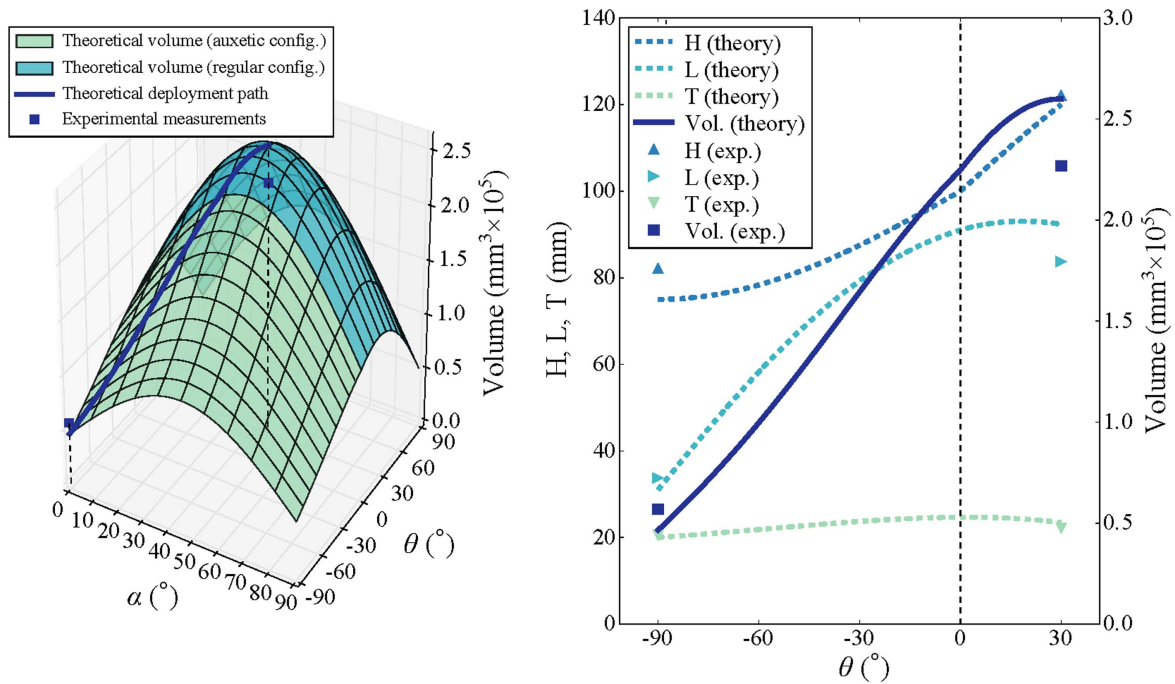
Figure 8. Experimental results versus analytical predictions for honeycomb deployment. Left: a surface plot showing the theoretical volume in α, θ space. The line shows the predicted volume change during deployment according to the analytical models. The blue squares represent the measured volume of the honeycomb's stowed and deployed states. Right: the variation of the individual honeycomb dimensions with α and θ (only θ shown on the x-axis).

more material was consumed in the strip folds than initially expected. In the deployed configuration, the honeycomb expanded fully in the H-direction but not completely in the L-direction. It is worth mentioning that the thickness T was virtually unchanged after deployment, while the dimension H had a final measured $\approx 5\%$ difference from the theoretical prediction. The hinges did not provide a deployment as effective as the one observed in the strips, likely due to the different thicknesses of the components. As mentioned in section 2.2, the thickness of the hinge and the position of the neutral axis have a large effect on the opening moment generated by the hinge. This is supported by the fact that the strip folds (thickness between $t_1 = 2.5$ mm and $t_2 = 1.25$ mm) deployed fully while the hinge folds ($t_{\text{hinge}} = 1$ mm) did not. Furthermore, the SMP Kirigami honeycomb demonstrator showed the feasibility of the concept and the general validity of the geometric formulas for the deployment ratio.

From figure 8 we can see that the deployment path taken by our demonstrator goes from the minimum to the maximum possible volume. The minimum volume configurations correspond to starting α angles of $0°$ and $90°$, with a maximum starting volume at $\alpha = 45°$. For the hexagonal centresymmetric open honeycomb configuration used the maximum volume at deployment corresponds to an angle $\theta = 30°$. It is however worth noticing that, aside from the one adopted in this work, other possible paths (e.g. starting from a different corner of the design envelope) are possible. This shows that the shape change exhibited by our demonstrator is by no means the only possible motion, and different geometries and SMP materials with multiple activation temperatures could produce different results. The current volumetric or stowage

deployment ratio is 5.2 (figure 8), but the theoretical volume surface is based on the fixed honeycomb dimensions used in this work. By changing these dimensions we could achieve an even greater volume change, or we could optimise the honeycomb for a specific task—e.g. deployment along a certain direction.

4. Conclusions

We have manufactured a working demonstrator to test the feasibility of using SMPs to actuate the folds in open Kirigami honeycombs. The concept shown in this paper builds on previous work, to create a model which takes into account the thickness of the honeycomb cell walls. The moment activation can be controlled through the geometry of the hinge and the tupe of shape memory material used. The model shows good agreement with the deployment experiment. In this work we chose our honeycomb configuration to have the largest possible ratio of stowed to deployed volume, but in principle one could optimise the configuration for a specific application or use with different SMPs. For more complex structures, the recent work by Chen *et al* [53] could be used to model structures with hierarchical and sequential folds.Though the demonstrator successfully deployed, there is room for improvement. While the hinge moment generated by the SMP was large enough to overcome friction and deploy the honeycomb, it is currently very low for practical purposes and would not be suitable for larger structures. The hinge design could be significantly improved by including a paper layer to offset the SMP further from the neutral axis and make it more mechanically effective.

A paper-SMP laminate manufacturing method could also allow us to better control the hinges' range of motion and design more complex Kirigami mechanisms.

Acknowledgments

References

[1] Miura K, Furuya H and Suzuki K 1985 Variable geometry truss and its application to deployable truss and space crane arm *Acta Astronaut.* **12** 599–607
[2] Tachi T 2009 One-dof cylindrical deployable structures with rigid quadrilateral panels *Proc. IASS Symp. (October)* pp 2295–305 (http://riunet.upv.es/handle/10251/7277)
[3] Schenk M, Kerr S G, Smyth a M and Guest S D 2013 Inflatable cylinders for deployable space structures *Proc. First Conference Transformables 2013 (School of Architecture Seville, Spain, 18–20 September 2013)*
[4] Miura K 2009 Triangles and quadrangles in space *50th Evolution and Trends in Design, Analysis and Construction of Shell and Spatial Structures: Proc. Symp. of the Int. Association for Shell and Spatial Structures (Valencia, October 2009)* pp 27–38 (https://riunet.upv.es/handle/10251/6461)
[5] Schenk M and Guest S D 2010 Folded textured sheets *Proc. Int. Association for Shell and Spatial Structures (IASS) Symp.* October) pp 2328–36 (http://riunet.upv.es/handle/10251/7280)
[6] Zhou X, Wang H and You Z 2014 Mechanical properties of Miura-based folded cores under quasi-static loads *Thin-Walled Struct.* **82** 296–310
[7] Kuribayashi K, Tsuchiya K, You Z, Tomus D, Umemoto M, Ito T and Sasaki M 2006 Self-deployable origami stent grafts as a biomedical application of Ni-rich TiNi shape memory alloy foil *Mater. Sci. Eng.* A **419** 131–7
[8] Bassik N, Stern G M and Gracias D H 2009 Microassembly based on hands free origami with bidirectional curvature *Appl. Phys. Lett.* **95** 1–4
[9] Balkcom D J and Mason M T 2008 Robotic origami folding *Int. J. Robot. Res.* **27** 613–27
[10] Cranford S, Sen D and Buehler M J 2009 Meso-origami: folding multilayer graphene sheets *Appl. Phys. Lett.* **95** 2013–6
[11] Tachi T 2010 Geometric considerations for the design of rigid origami structures *Proc. Int. Association for Shell and Spatial Structures (IASS) Symp. 2010* vol 12, pp 458–60
[12] Wu Q, Yu F, Okabe Y, Saito K and Kobayashi S 2015 Acoustic emission detection and position identification of transverse cracks in carbon fiber-reinforced plastic laminates by using a novel optical fiber ultrasonic sensing system *Struct. Health Monit.* **14** 205–13
[13] Guest S D and Pellegrino S 1994 The folding of triangulated cylinders: I. Geometric considerations *J. Appl. Mech.* **61** 773

[14] Dacorogna B, Marcellini P and Paolini E 2010 *Origami and Partial Differential Equations* vol 57 (Milan: Springer) pp 598–606
[15] Sun J, Scarpa F, Liu Y and Leng J 2015 Morphing thickness in airfoils using pneumatic flexible tubes and Kirigami honeycomb *J. Intell. Mater. Syst. Struct.* **27** 755–63
[16] Sareh S and Rossiter J 2013 Kirigami artificial muscles with complex biologically inspired morphologies *Smart Mater. Struct.* **22** 014004
[17] Zhang Y *et al* 2015 A mechanically driven form of Kirigami as a route to 3D mesostructures in micro/nanomembranes *Proc. Natl Acad. Sci.* **112** 201515602
[18] Virk K, Monti A, Trehard T, Marsh M, Hazra K, Boba K, Remillat C D L, Scarpa F and Farrow I R 2013 SILICOMB PEEK Kirigami cellular structures: mechanical response and energy dissipation through zero and negative stiffness *Smart Mater. Struct.* **22** 084014
[19] Pflug J and Neirinck W 2008 Elastic honeycomb sheet, its production process and equipment to produce *Patent* WO 2008/141688 A2
[20] Hou Y, Neville R M, Scarpa F, Remillat C, Gu B and Ruzzene M 2014 Graded conventional-auxetic Kirigami sandwich structures: flatwise compression and edgewise loading *Composites* B **59** 33–42
[21] Scarpa F, Ouisse M, Collet M and Saito K 2013 Kirigami auxetic pyramidal core: mechanical properties and wave propagation analysis in damped lattice *J. Vib. Acoust.* **135** 041001
[22] Ouisse M, Collet M and Scarpa F 2016 A piezo-shunted kirigami auxetic lattice for adaptive elastic wave filtering *Smart Mater. Struct.* **25** 115016
[23] Blees M K *et al* 2015 Graphene kirigami *Nature* **524** 204–7
[24] Shyu T C, Damasceno P F, Dodd P M, Lamoureux A, Xu L, Shlian M, Shtein M, Glotzer S C and Kotov N A 2015 A kirigami approach to engineering elasticity in nanocomposites through patterned defects *Nat. Mater.* **14** 785–9
[25] Xu L, Wang X, Kim Y, Shyu T C, Lyu J and Kotov N A 2016 Kirigami nanocomposites as wide-angle diffraction gratings *ACS Nano* **10** 6156–62
[26] Dean H B 1921 Artificial honeycomb *Patent* US 1,389, 294
[27] Nojima T and Saito K 2006 Development of newly designed ultra-light core structures *JSME Int. J. Ser.* A **49** 38–42
[28] Saito K, Pellegrino S and Nojima T 2014 Manufacture of arbitrary cross-section composite honeycomb cores based on origami techniques *J. Mech. Des.* **136** 051011
[29] Neville R M, Pirrera A and Scarpa F 2014 Open shape morphing honeycombs through kirigami *SMASIS 2014: Proc. ASME 2014 Conf. on Smart Materials, Adaptive Structures and Intelligent Systems (Newport, RI)*
[30] Neville R M, Scarpa F and Pirrera A 2016 Shape morphing Kirigami mechanical metamaterials *Sci. Rep.* **6** 31067
[31] Liu C, Qin H and Mather P T 2007 Review of progress in shape-memory polymers *J. Mater. Chem.* **17** 1543
[32] Li P, Yan Z, Zhang L, Liu Y, Leng J and Lau K T 2013 Monitoring of deployment process of shape memory polymers for morphing structures with embedded fibre Bragg grating sensors *J. Intell. Mater. Syst. Struct.* **25** 1224–32
[33] John M and Li G 2010 Self-healing of sandwich structures with a grid stiffened shape memory polymer syntactic foam core *Smart Mater. Struct.* **19** 075013
[34] Du H, Liu L, Leng J, Peng H, Scarpa F and Liu Y 2015 Shape memory polymer s-shaped mandrel for composite air duct manufacturing *Compos. Struct.* **133** 930–8
[35] Yang Y, Chen Y, Wei Y and Li Y 2016 3d printing of shape memory polymer for functional part fabrication *Int. J. Adv. Manuf. Technol.* **84** 2079–95

[36] Butaud P, Ouisse M, Placet V and Foltête E 2014 Experimental investigations on viscoelastic properties of a shape memory polymer *ASME 2014 Conf. on Smart Materials, Adaptive Structures and Intelligent Systems*

[37] Hassan M R, Scarpa F and Mohamed N A 2004 Shape memory alloys honeycomb: design and properties *Proc. SPIE* **5387** 557–64

[38] Grummon D S, Shaw J A and Foltz J 2006 Fabrication of cellular shape memory alloy materials by reactive eutectic brazing using niobium *Mater. Sci. Eng.* A **438–440** 1113–8 *Proc. Int. Conf. on Martensitic Transformations*

[39] Shaw J, Churchill C, Triantafyllidis N, Michailidis P, Grummon D and Foltz J 2007 Shape memory alloy honeycombs: experiments and simulation *48th AIAA/ASME/ASCE/AHS/ASC Structures, Structural Dynamics, and Materials Conf.* 2016/12/20 (https://doi.org/10.2514/6.2007-1739)

[40] Hassan M R, Scarpa F, Mohamed N A and Ruzzene M 2008 Tensile properties of shape memory alloy chiral honeycombs *Phys. Status Solidi* b **245** 2440–4

[41] Michailidis P, Triantafyllidis N, Shaw J and Grummon D 2009 Superelasticity and stability of a shape memory alloy hexagonal honeycomb under in-plane compression *Int. J. Solids Struct.* **46** 2724–38

[42] Hassan M, Scarpa F, Ruzzene M and Mohammed N 2008 Smart shape memory alloy chiral honeycomb *Mater. Sci. Eng.* A **481–482** 654–7

[43] Jacobs S, Coconnier C, DiMaio D, Scarpa F, Toso M and Martinez J 2012 Deployable auxetic shape memory alloy cellular antenna demonstrator: design, manufacturing and modal testing *Smart Mater. Struct.* **21** 075013

[44] Rossiter J, Takashima K, Scarpa F, Walters P and Mukai T 2014 Shape memory polymer hexachiral auxetic structures with tunable stiffness *Smart Mater. Struct.* **23** 045007

[45] Lakes R 1987 Foam structures with a negative Poisson's ratio *Science* **235** 1038–40

[46] Evans K E and Alderson A 2000 Auxetic materials: functional materials and structures from lateral thinking! *Adv. Mater.* **12** 617–28

[47] Hawkes E, An B, Benbernou N M, Tanaka H, Kim S, Demaine E D, Rus D and Wood R J 2010 Programmable matter by folding *Proc. Natl Acad Sci. USA* **107** 441–5

[48] Felton S M, Tolley M T, Shin B, Onal C D, Demaine E D, Rus D and Wood R J 2013 Self-folding with shape memory composites *Soft Matter* **9** 7688

[49] Tolley M T, Felton S M, Miyashita S, Aukes D, Rus D and Wood R J 2014 Self-folding origami: shape memory composites activated by uniform heating *Smart Mater. Struct.* **23** 094006

[50] Zhao Q, Zou W, Luo Y and Xie T 2016 Shape memory polymer network with thermally distinct elasticity and plasticity *Sci. Adv.* **2** e1501297

[51] Young W C and Budnyas R G 2002 *Roark's Formulas for Stress and Strain* 7th edn (New York: McGraw-Hill)

[52] Zhang D, Liu Y, Yu K and Leng J 2011 Influence of cross-linking agent on thermomechanical properties and shape memory effect of styrene shape memory polymer *J. Intell. Mater. Syst. Struct.* **22** 2147–54

[53] Chen Y, Peng R and You Z 2015 Origami of thick panels *Science* **349** 396–400